RSC Advances

PAPER

View Article Online
View Journal | View Issue

Cite this: *RSC Adv.*, 2024, **14**, 27883

Effect of pyrolysis temperature on physicochemical characteristics and toxic elements for grub manure-derived biochar†

Qingsong Zhao,[ab] Jiayi Cui,[a] Yuxin Hou[a] and Penggang Pei *[abc]

While traditional solutions for disposing of animal manure are limited by their time-consuming nature and inefficiency, the pyrolysis of animal manure into biochar is considered a promising disposal option, offering high-value benefits. However, there are few research studies on the physicochemical properties and potential utilization pathway of grub manure-derived biochar (GB) prepared at different temperatures. In this study, grub manure (GM) was pyrolyzed at 450, 600 and 750 °C, and the effect of pyrolysis temperature on the characteristics and applications of GB was illustrated. The results showed that increasing pyrolysis temperature promoted the formation of an aromatic structure, enhanced the stability, and improved the surface pore structure of GB. The relationship between pyrolysis temperature and C/N-containing functional groups in GB was quantitatively analyzed. In the process of pyrolysis of GM to GB, carbonates first decomposed, and then, C=O broke into C–O and finally condensed to form an aromatic ring structure at elevated pyrolysis temperature. Although GM was rich in organic matter and total N/P/K, the potentially toxic elements (PTEs) (Ni, Cu, Cd, Pb, Zn and As) in GM presented potential risk. The hazard of PTEs in GB was significantly decreased after GM was pyrolyzed. Overall, pyrolysis provided an opportunity for the sustainable management of GM, and GB is a multi-purpose and high-value product that could be applied in soil improvement, environmental remediation, and climate change mitigation for achieving sustainable development.

Received 22nd May 2024
Accepted 19th August 2024

DOI: 10.1039/d4ra03778b

rsc.li/rsc-advances

1 Introduction

Protaetia brevitarsis Lewis is an important agricultural pests, widely distributed in China and neighbouring countries. Its larvae, commonly called grubs, are scavengers, mainly feeding on rotten straw, animal manure and livestock waste, and are not harmful to plants as well as have great exploitation value.[1] A previous study showed that feeding grubs with spent mushroom substrates could produce a high-value product (mature grubs), which is rich in high-quality protein and fat components and traditional medicinal material.[2] In additional, Li *et al.*[3] have reported that the content of humic acids in grub manure (GM) produced by the biological transformation of maize straw and sawdust by grubs reached 24.37% and 14.46%, respectively. Xuan *et al.*[4] found that the potential microbial community in GM improved the soil environment, and the colonization of some beneficial microorganisms (*Bacillus*) enhanced plant disease resistance and thus promoted plant growth. Moreover, Joung *et al.*[5] indicated that the application of GM with chemical fertilizers significantly increased the content of soil organic matter and the yield of lettuce by 114–186% and 9.16–19.96%, respectively, compared with the application of chemical fertilizers. Therefore, GM is an excellent precursor or substrate for agronomic or environmental applications. However, in recent years, the study on the application of GM is still in the early stage, and it is mainly returned to the field directly. Therefore, further research on the deep exploitation of GM is required.

Aerobic composting and anaerobic digestion are traditional measures to dispose of animal manure. Compost using manure has long duration and possibly instigates potentially toxic element leaching risk.[6] Under a hypoxic environment, although anaerobic digestion converts manure to biogas (mainly CO_2 and CH_4), it is also accompanied with the emission of pungent gases (H_2S and NH_3).[7] In recent years, thermochemical conversion has attracted widespread attention as a promising technology for converting biomass to value-added products. Biochar (BC), as the most attractive product, has shown developing potential in climate change mitigation, contamination remediation, soil improvement and fertilizers, and energy storage.[8–10] The multiple structures and function of BC are related to the preparation conditions, especially pyrolysis temperature. Yan *et al.*[11]

[a]*Department of Life Sciences, Changzhi University, Changzhi, China. E-mail: ppg140425@126.com; Tel: (+86) 0355-2178331*

[b]*Shanxi Province Engineering Research Center of Soil Microbial Remediation Technology, China*

[c]*Key Laboratory of Original Agro-Environmental Pollution Prevention and Control, Ministry of Agriculture and Rural Affairs (MARA), Agro-Environmental Protection Institute, Tianjin, China*

† Electronic supplementary information (ESI) available. See DOI: https://doi.org/10.1039/d4ra03778b

showed that the pore structure of chicken manure BC was developed as the pyrolysis temperature increased. Zhang *et al.*[12] indicated that the ash content, pH value and specific surface area of cow manure increased, and the content of nitrogen, oxygen, carboxyl and phenolic hydroxyl decreased at elevated pyrolysis temperature. Wei *et al.*[13] prepared pig manure BC at 300–700 °C, and found that the pig manure BC produced at high temperature possessed high carbon stability. To date, the physicochemical properties of most animal manure-derived biochar have been reported, whereas the research on the characteristics of grub manure-derived biochar (GB) is relatively limited. More importantly, quantitative analysis of the effect of pyrolysis temperature on the properties of GB in order to precisely predict its application in future is needed.

Although BC has excellent structural properties and a wide range of applications, environmental hazards of potentially toxic elements (PTEs) in BC should be considered.[14] A previous study showed that the content of As, Cu, Mo and Zn was concentrated in BC when dairy manure was pyrolyzed at 700 °C.[15] However, pyrolysis can effectively immobilize PTEs in pig and cow manure, and the bioavailable fraction of PTEs was transformed to a relatively stable fraction at elevated temperature.[16,17] Hence, it is necessary to analyze and evaluate the potential risk of PTEs in GBs. In this study, grub manure-derived BCs were produced at 450, 600 and 750 °C. The elemental composition, microstructure feature, thermal stability, crystal structure and surface functionality of GBs were systematically explored by advanced characterization techniques. Moreover, the total content, leachable concentration, chemical fraction, and potential environmental risk of PTEs in GBs were comprehensively analyzed. In addition, the underlying application of GB produced at different temperatures was discussed. This study is expected to scientifically explain the pyrolysis mechanism of grub manure, and provide comprehensive and detailed information for the preparation and application of grub manure biochar.

2 Materials and methods

2.1 Biochar preparation

Grub manure (GM), collected from Changzhi in Shanxi province, China, was used in this work. The GM was air-dried at 40 °C for 24 h to remove the moisture, and then dried GM was ground, smashed and sieved through a 0.25 mm sieve. Since the BC prepared at low temperature underwent incomplete combustion, and we referred to a previous research scheme,[18] the pyrolysis temperature was selected as 450–750 °C in this study. The GM (20 g) was pyrolyzed in a tube furnace at 450, 600 and 750 °C under a N_2 atmosphere for 2 h with a heating rate of 15 °C min^{-1}. After pyrolysis, the grub manure-derived biochar (GB) was collected, homogenized and stored for further characterization. The schematic diagram of the experiment is indicated in Fig. 1.

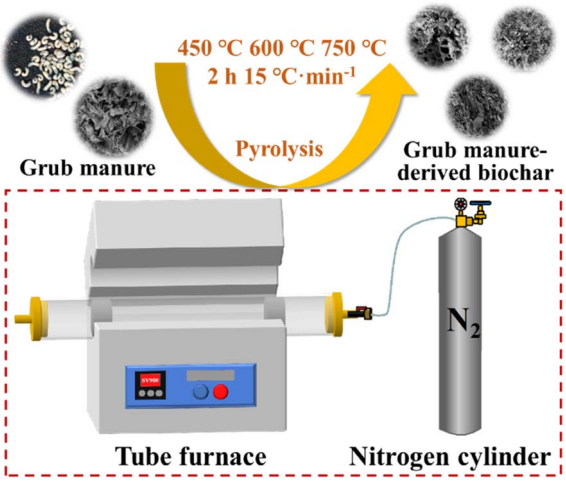

Fig. 1 A schematic of the experiment.

2.2 Grub manure and grub manure-derived biochar characterization

The ultimate analysis of carbon (C), hydrogen (H), nitrogen (N), sulfur (S) and oxygen (O) in GM and GBs was performed using a CHNS/O elemental analyzer (EA3000, Jena, Germany). The ash content of GM and GBs was determined by heating at 550 °C for 4 h in a muffle furnace. The solid organic matter (SOM) of GM and GBs was determined by the potassium dichromate oxidation volumetric method. The samples were digested with H_2SO_4 and H_2O_2, and the total phosphate (TP) and total potassium (TK) of GM and BCs were measured by the vanadium molybdate yellow colorimetric method, and flame spectrometry method.[19] The N_2 adsorption–desorption curve of GM and GB was measured using an ASAP 2460 (Micromeritics, USA) at 77 K. The samples were degasified in a vacuum for 12 h at 300 °C. The specific surface area, total pore volume and average pore diameter of GM and BCs were calculated based on Brunauer–Emmett–Teller (BET) and Barrett–Joyner–Halenda (BJH) methods. The surface morphology and element distribution of GM and GBs were characterized using scanning electron microscopy coupled with energy dispersive spectroscopy (SEM-EDS) (S-4800, Hitachi, Japan). The figure was captured in high vacuum conditions and the acceleration voltage was between 5 and 15 kV. The thermogravimetry (TG) and derivative thermogravimetry (DTG) curves of GM and BCs were studied using a NETZSCH STA 449F5 Jupiter (NETZSCH, Germany). The samples were heated from 20 °C to 900 °C at a heating rate of 10 °C min^{-1} and under a N_2 atmosphere with a flow rate of 20 mL min^{-1}. The crystallography of GM and GBs was determined using X-ray Powder Diffraction (XRD) (X'Pert Pro MPD, Holland analytical, Netherlands) with a Cu Kα source at 5–80° at a scanning rate of 8° min^{-1}.

The structural properties of GM and GBs were evaluated using solid state ^{13}C nuclear magnetic resonance (^{13}C-NMR) spectroscopy (Bruker 400M, Germany), Raman spectroscopy (RM2000, Renishaw, UK) and X-ray photoelectron spectroscopy (XPS) (ESCALAB 250XI, Thermo Scientific, USA). The ^{13}C-NMR spectra were recorded at a frequency of 100.6 MHz with a spinning speed of 5 kHz. The Raman spectra of samples were scanned with a laser power of 15 mW, excitation line of 532 nm, and spectral range of 100–400 cm^{-1}. XPS was performed at 15 kV and 10 mA with a 500 μm diameter beam of Al Kα X-rays (*hν*

= 1486.8 eV). The surface functional groups of GM and BCs were obtained by Fourier transform infrared spectroscopy (FTIR) (Nicolet iS10, Thermo Scientific, USA). The sample was co-ground with grades KBr (1 : 100, m/m) and the signal was recorded for 32 times at a step of 4 cm^{-1} between the wavenumbers of 4000 and 400 cm^{-1}. The two-dimensional correlation spectrum was used to analyze the FTIR data using 2DShige software.

The GM and GBs (0.2500 g) were digested with HF (5 mL) and HNO_3 (8 mL) at 120 °C for 1 h and 150 °C for 2 h, and the total potentially toxic element (PTE) content of samples was determined by inductively coupled plasma mass spectrometry (ICP-MS) (iCAP Q, USA). Based on a pervious study,[20] the leachability of PTEs in BM and BC was assessed using the toxicity characteristic leaching procedure (TCLP), and the risk evaluation index (REI) was used to evaluate the ecological risk of PTEs in GM and GBs. The PTE fractions of GM and GBs were determined using the sequential extraction method based on Tessier *et al.*[21] Briefly, the speciation of potentially toxic elements in GM and GBs were divided into the exchangeable (EXC), carbonate bound (CAR), Fe–Mn oxide bound (OX), organic matter bound (OM), and residual (RES) fractions. The EXC, CAR, OX and OM fractions of PTEs were extracted by using 1.0 M $MgCl_2$ solution, 1.0 M NaOAc-HOAc solution, 0.04 M NH_4OH–HCl in 25% HOAc, and 0.02 M HNO_3-30% H_2O_2 and 3.2 M NH_4OAc respectively. The RES fraction of PTEs was digested by HF–HNO_3 and was analyzed using ICP-MS. The quality assurance and quality control (QA/QC) was performed using duplicate samples with three replicates, blanks, and standard reference materials (NIST 2586) with the recovery of 95–105%. In the process of test, the blank and standard reference samples were measured every 15 samples for QA/QC data.

2.3 Statistical analysis

All the experiments were performed in triplicate. The significant difference among the properties of GM and GBs, and the relationships between pyrolysis temperature and GB properties were evaluated using one-way analysis of variance and regression analysis (IBM SPSS 25, USA), respectively.

3 Results and discussion

3.1 Elemental composition

As shown in Table 1, the carbon (C) and oxygen (O) content in grub manure was rich, reaching 33.35% and 32.96%, respectively. For all GB, the C content was highest (32.49–35.10%), followed by O (11.71–19.49%). With increasing the pyrolysis temperature, the C and O content in GB decreased significantly, which resulted from the loss of volatile matter and the decomposition of unstable organic matter under high temperature.[22] Similarly, the H content in GB significantly decreased compared to the feedstock. The atomic ratio H/C and O/C of GB was lower than that of GM, and that of GB decreased at elevated pyrolysis temperature. These results indicated that GB underwent dehydration and depolymerization reaction, and the aromaticity and stability of GB were enhanced with increasing the pyrolysis temperature.[23] The double bond equivalents and aromaticity index of GB increased as the temperature elevated, which confirmed the formation of condensed aromatic structures at high temperature. The ash content of GM was 26.51%. After pyrolysis, the ash content of GB1, GB2 and GB3 was 40.97%, 46.87% and 53.24, respectively. The ash content of GB increased as the pyrolysis temperature increased, which was attributed to the concentration and accumulation of mineral elements.[24]

The nutrient content of BC determines its agricultural application. In this study, the SOM, TN, TP and TK contents of GM and GB were detected (Table 1). The SOM, TN, TP and TK content of GB was 51.75%, 2.45%, 0.87% and 0.29%. Similarly, Mishra *et al.* reported that neem seed BC is also rich in nutrients,[25] which suggested that GB could be used to enhance soil nutrition and improve soil structure.[26] After pyrolysis, the SOM, TN and TP of GB significantly decreased to 36.88–49.54%, 1.17–2.29% and 0.26–0.30%, respectively, and the TK content increased to 0.48–0.56%, which were similar to the results of sewage sludge BC.[27]

3.2 Microstructure feature

The surface morphology and elemental distribution of GM and GBs are exhibited in Fig. 2. The surface of GM was rough and showed irregular pores. When GM was pyrolyzed at 450–600 °C, the dehydration process and release of volatile matter from the C skeleton facilitated the formation of a BC surface pore structure. As the pyrolysis temperature increased to 750 °C, more micro-pore structures were developed in the GB surface. At high pyrolysis temperature, the amorphous C (aromatic and aliphatic forms) in GB were converted to graphite crystallites, and the graphene sheets were denser than the former, so this phase conversion resulted in the generation of fine-pore structures.[23] The EDS mapping revealed that C and O on the GB surface were abundant and uniformly distributed. In addition, the Ca and K signals of the GB surface were enhanced at elevated pyrolysis temperature.

The N_2 adsorption–desorption curves of GM and GBs are shown in Fig. S1.† The observed isotherm of samples was a type IV isotherm, which suggested that the surface of GM and GBs was mainly a mesoporous structure.[18] The quantitative analysis of pore structure of GM and GBs is shown in Table 1. The specific surface area (SSA), total pore volume (TPV), and average pore diameter (APD) of GM were 5.87 $m^2\ g^{-1}$, 0.02 $cm^3\ g^{-1}$ and 10.81 nm, respectively. When the pyrolysis temperature rose from 450 °C to 600 °C, pore structures were developed on the surface of GB, and the SSA and TPV gradually increased compared with feedstock. With the pyrolysis temperature rising to 750 °C, the SSA and TPV of GB increased sharply, reaching 98.68 $m^2\ g^{-1}$ and 0.10 $cm^3\ g^{-1}$. As described in the result of SEM images, the surface pore diameter of GB first enlarged and then decreased with increasing pyrolysis temperature. Compared to GB produced at 450 °C, the APD of GB produced at 600 °C increased from 12.09 nm to 17.81 nm. The APD of GB prepared at 750 °C decreased to 4.08 nm. A similar result was reported in a previous study, where Zhao *et al.* observed that the APD of

Table 1 Characteristics of grub manure (GM) and grub manure-derived biochar (GB)[a]

Property	GM	GB1	GB2	GB3
C (%)	33.35 ± 0.12c	35.10 ± 0.13a	33.91 ± 0.07b	32.49 ± 0.04d
O (%)	32.96 ± 0.04a	19.49 ± 0.1b	15.75 ± 0.09c	11.71 ± 0.15d
H (%)	4.10 ± 0.06a	1.77 ± 0.12b	1.11 ± 0.03c	0.98 ± 0.02d
S (%)	0.63 ± 0.14a	0.38 ± 0.04b	0.39 ± 0.02b	0.41 ± 0b
Ash (%)	26.51 ± 0.18d	40.97 ± 0.43c	46.87 ± 0.1b	53.24 ± 0.19a
Atomic ratio H/C	1.47 ± 0.02a	0.60 ± 0.04b	0.39 ± 0.01c	0.36 ± 0.01c
Atomic ratio O/C	0.74 ± 0a	0.42 ± 0b	0.35 ± 0c	0.27 ± 0d
DBE	0.33 ± 0.01a	0.76 ± 0.02b	0.86 ± 0c	0.87 ± 0c
AI	0a	0.63 ± 0.03b	0.83 ± 0c	0.85 ± 0c
SOM (%)	51.75 ± 0.18a	49.54 ± 0.15b	44.50 ± 1.25c	36.88 ± 0.48d
TN (%)	2.45 ± 0.08a	2.29 ± 0.1b	1.98 ± 0.08c	1.17 ± 0.01d
TP (%)	0.87 ± 0.01a	0.30 ± 0.01b	0.26 ± 0.01c	0.29 ± 0.01b
TK (%)	0.29 ± 0.01c	0.48 ± 0.02b	0.52 ± 0.04 ab	0.56 ± 0.01a
SSA (m^2 g^{-1})	5.87 ± 0.12 c	6.79 ± 0.28b	6.64 ± 0.31b	98.68 ± 0.91a
TPV (cm^3 g^{-1})	0.02 ± 0.001 d	0.03 ± 0.001c	0.04 ± 0.001b	0.10 ± 0.002a
APD (nm)	10.81 ± 0.20 c	12.09 ± 0.51b	17.81 ± 0.11a	4.08 ± 0.35d

[a] Data are shown as mean ± standard deviation ($n = 3$). GB1, GB2 and GB3 represent grub manure-derived biochar produced at 450, 600 and 750 °C, respectively. TN: total nitrogen. TP: total phosphate. TK: total potassium. SOM: solid organic matter. DBE: double bond equivalents. AI: aromaticity index. SSA: specific surface area. TPV: total pore volume. APD: average pore diameter. Different letters indicate significant differences between different treatments ($P < 0.05$).

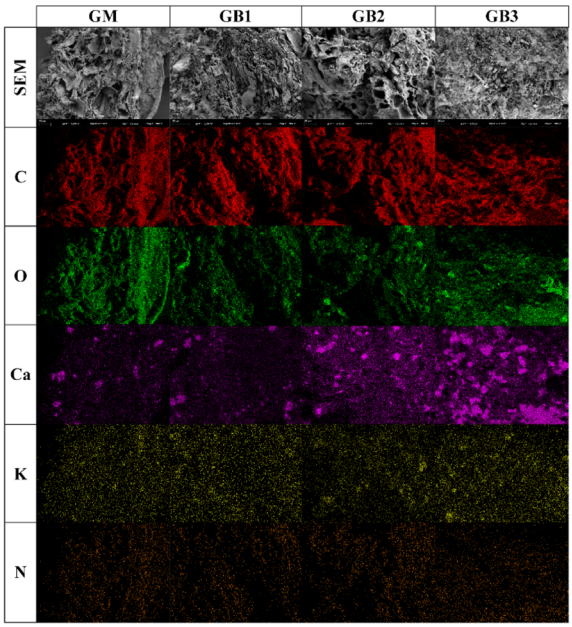

Fig. 2 The scanning electron microscopy and energy dispersive spectroscopy (SEM-EDS) mapping of grub manure (GM) and grub manure-derived biochar (GB). GB1, GB2 and GB3 represent grub manure-derived biochar produced at 450, 600 and 750 °C, respectively.

rapeseed stem derived BC decreased at elevated pyrolysis temperature.[28] The formation of smaller diameter pores resulted from that greater amounts of labile and volatile matter were removed under high pyrolysis temperature.[29] According to the APD of GB, it could be shown that GBs (produced at 450–750 °C) are mesoporous materials.[30] Overall, the GB prepared at 750 °C possessed an excellent pore structure, which indicated that GB (750 °C) could be applied in environmental remediation as an adsorbent or catalyst.[31]

3.3 Thermal stability

The thermal degradation performance of the GM and GBs is shown in Fig. 3a and b. The feedstock showed five mass loss peaks. The first weight loss peak (at 65 °C) of GM was associated with the release of moisture. At approximately 161 °C, the degradation of volatile matter resulted in the reduction of GM weight. The GM had an obvious weight loss peak at 361 °C which was related to the thermal decomposition reaction of the organics (protein and carbohydrate).[32] The fourth weight loss peak for GM at around 499 °C represented the decomposition of fixed carbon. From 650 °C to 750 °C, the GM and GBs all exhibited a significant weight loss peak, which resulted from the dehydrogenation and the decomposition of calcite ($CaCO_3$).[33] Overall, the final residual weight of GM and GBs was 33.97% and 69.95–85.65%, respectively. Specifically, the residual weight of GB increased with the increase of pyrolysis temperature, which indicated the improvement of its thermal stability.

3.4 Crystal structure

The crystal structure of GM before and after pyrolysis was characterized using XRD, and the results are shown in Fig. 3c. There were two types of crystalline phases in GM. The diffraction reflection at $2\theta = 26.65°$ indicated the presence of quartz (SiO_2, PDF No. 46-1045), and those at $2\theta = 14.96°$, 24.44°, 38.37° and 50.25° were indicative of whewellite ($CaC_2O_4 \cdot H_2O$, PDF No. 20-0231). When GM was pyrolyzed at 450 °C and 600 °C, the reflection of whewellite disappeared, and the diffraction peak of calcite ($CaCO_3$, PDF No. 47-1743) appeared at $2\theta = 29.42°$, 39.42°, and 43.27°. This indicated that $CaC_2O_4 \cdot H_2O$ was

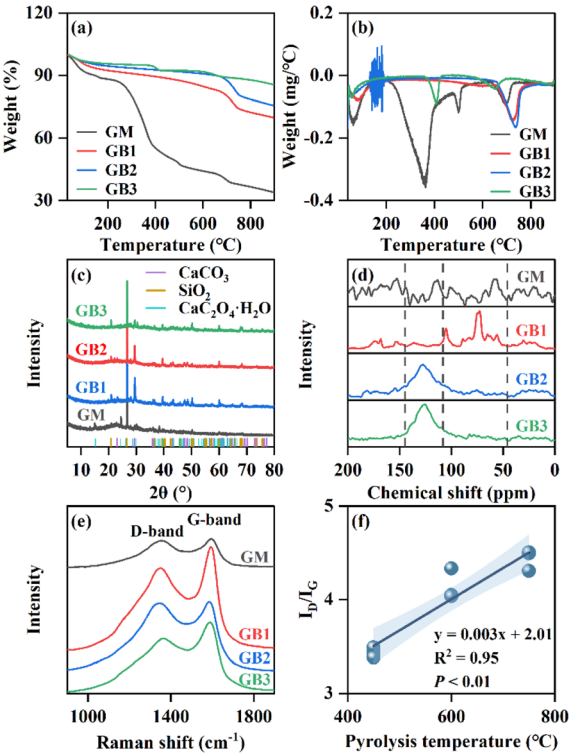

Fig. 3 The thermogravimetric (a) and derivative thermogravimetric (b) curves of GM and GB. The XRD pattern of GM and GB (c). The ^{13}C-NMR spectra of GM and GB (d). The Raman spectra of GM and GB (e), and the line regression analysis of pyrolysis temperature and the area ratio of the D-band and G-band (I_D/I_G) (f). GM and GB indicate grub manure and grub-derived biochar, respectively. GB1, GB2 and GB3 represent grub manure-derived biochar produced at 450, 600 and 750 °C, respectively.

decomposed to $CaCO_3$ during the pyrolysis process of GM. When the pyrolysis temperature rose to 750 °C, the intensity of the $CaCO_3$ peak in GB3 decreased, suggesting the thermal decomposition of $CaCO_3$ in GB with increasing pyrolysis temperature.

3.5 Surface functionality

^{13}C-NMR was used to elucidate the surface functional groups of GM and GBs (Fig. 3d). The GM exhibited dominant peaks at 0–46, 46–65, 108–145, and 160–185 ppm, which indicated the presence of alkyl-C, aliphatic-C, aromatic/phenolic-C, and carboxyl-C in GM.[34] The typical peaks of aliphatic-C and *O*-alkyl-C were observed in the spectral region of 46–90 ppm for GB produced at 450 °C. As the pyrolysis temperature increased, the intensity of aliphatic-C in GB decreased and that of aromatic-C (region of 108–145 ppm) enhanced. The spectra of GB pyrolyzed at high temperature (GB2 and GB3) revealed a representative aromatic-C peak. Similar results have been reported by Sun *et al.*,[35] who suggested that the aliphatic compounds in GB underwent thermal decomposition and converted to an aromatic cluster structure at elevated pyrolysis temperature. In summary, the aromaticity of GB pyrolyzed at high temperature was high, which showed that it could act as a means for promoting carbon sequestration.

Raman spectra were employed to characterize the C structure and quantitively evaluate the structural defects in BC.[36] The Raman spectra of GM and GBs showed a typical D-band (1357 cm^{-1}) and G-band (1595 cm^{-1}) (Fig. 3e), which were associated with the defect structure and in-plane vibrations of sp^2 graphitic C, respectively. The area ratio of the D-band and G-band (I_D/I_G) was proportional to the defect and graphitic degree of carbon materials.[37] The I_D/I_G of GM was 2.77. After GM was pyrolyzed, the I_D/I_G of GB produced at 450, 600 and 750 °C was 3.44, 4.14 and 4.44, respectively. Importantly, the carbonization temperature (T) was significantly positively correlated with the I_D/I_G of GB (Fig. 3f), and the quantitative relationship was shown as $I_D/I_G = 0.003 \times T + 2.01$ ($R^2 = 0.95$, $P < 0.01$). These results suggested that the graphitic and defect degree of GM-derived BC was improved when GM was prepared at high pyrolysis temperature, which was consistent with the previous study.[38] These findings also indicated that GM-derived BCs have promising potential as adsorbents for wastewater treatment.[39,40]

The chemical states of C and N in GM and GBs were determined using XPS spectra. As shown in Fig. 4a–d, the C 1s spectra of GM and GB were deconvoluted into three peaks located at approximately 289.4, 286.1 and 284.8 eV, respectively, which were assigned to C=O, C–O and C–C/C=H, respectively.[37,41] The relative content of C=O, C–O and C–C/C=C in GM was 15.17%, 27.18% and 57.65%, respectively. When GM was pyrolyzed at 450 °C, the relative abundance of C-containing functional groups in GB1 followed the order of C–C/C=C (48.73%) > C–O (36.19%) > C=O (15.09%). As the pyrolysis

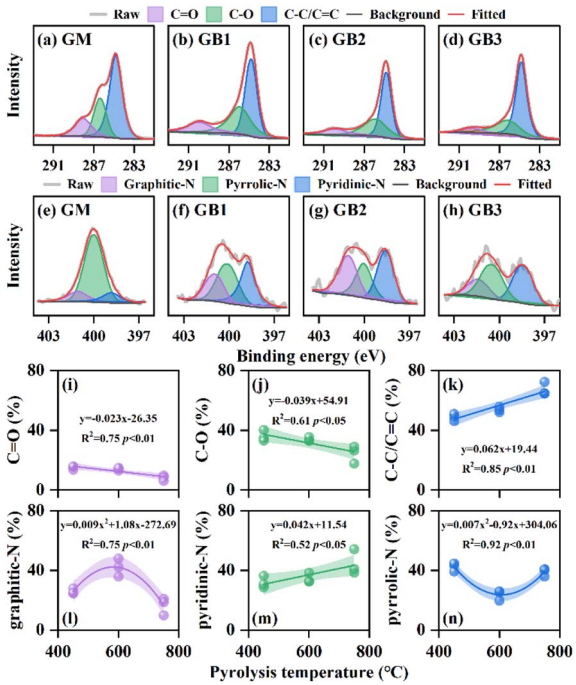

Fig. 4 The XPS spectra of C 1s (a–d) and N 1s (e–h) for GM and GB. The regression analysis of pyrolysis temperature and the relative content of functional groups (i–n). GM, GB1, GB2 and GB3 represent grub manure, and grub manure-derived biochar produced at 450, 600 and 750 °C.

temperature increased, the relative abundance of C–C/C=C significantly increased by 5.16–18.60%, and that of C–O and C–O gradually decreased by 2.18–11.67% and 3.00–6.94%, respectively. Fig. 4i–k demonstrated the quantitative correlation between the relative abundance of C-containing functional groups and pyrolysis temperature (450–750 °C), which was expressed as follows: C=O = $-0.023T - 26.35$ ($R^2 = 0.75$, $p < 0.01$), C–O = $-0.039T + 54.91$ ($R^2 = 0.61$, $p < 0.05$), and C–C/C=C = $0.062T + 19.44$ ($R^2 = 0.85$, $p < 0.01$).

The N 1s spectra of GM and GBs were assigned to graphitic-N (400.78–401.56 eV), pyrrolic-N (399.49–400.66 eV) and pyridinic-N (398.40–398.85 eV) (Fig. 4e–h).[42,43] The N-containing functional group in GM mainly existed in the form of pyrrolic-N (80.36%), while graphitic-N and pyridinic-N accounted for 12.37% and 7.27%, respectively. The relative content of graphitic-N and pyridinic-N in GBs increased by 4.17–29.57% and 24.57–37.25%, respectively, and that of pyrrolic-N decreased by 37.92–56.76% in GBs compared with GM. When the pyrolysis temperature rose from 450 to 600 °C, the five-member ring (pyrrolic-N) was converted to graphitic-N and pyridinic-N through condensation and polymerization.[44] With the increase of pyrolysis temperature, the graphitic-N was transformed to pyridinic-N and pyrrolic-N, which was in line with the previous research.[45] Furthermore, the numerical relationship between the relative abundance of N-containing functional groups and pyrolysis temperature was established and described as follows: graphitic-N = $0.009T^2 + 1.08T - 272.69$ (T = 450–750 °C, $R^2 = 0.75$, $p < 0.01$), pyridinic-N = $0.042T + 11.54$ (T = 450–750 °C, $R^2 = 0.52$, $p < 0.05$) and pyrrolic-N = $0.007T^2 - 0.92T + 304.06$ (T = 450–750 °C, $R^2 = 0.92$, $p < 0.01$).

The FTIR spectra of GM and GBs are shown in Fig. 5. The obvious peak at 3400 cm^{-1} is assigned to the stretching vibration of –OH on the surface of GM. The peak located at 2925 cm^{-1} is related to aliphatic groups (C–H) in GM. As the pyrolysis temperature increased, the abundance of –OH and C–H in GB gradually decreased, which was attributed to the cracking of organic matter in GM *via* dehydration and dehydrogenation reactions.[46] The band at 1624 cm^{-1} for GM belonged to C=O and the abundance of C=O in GB gradually decreased and disappeared at elevated temperature. This phenomenon indicated that C=O was cracked at high temperature by deoxygenation and decarbonization reaction.[47] The peak at 1428 cm^{-1} on the surface of GBs represented the out-of-plane bending of CO_3^{2-}, but was not present in GM. Meanwhile, the intensity of the CO_3^{2-} peak in GB reduced as the pyrolysis temperature increased. These were consistent with the results of XRD. When GM was pyrolyzed, the CaC_2O_4 in GM was converted to $CaCO_3$, and then $CaCO_3$ in GB was decomposed with the increase of pyrolysis temperature, which caused the CO_3^{2-} signal in FTIR for GB to first increase and then decrease at elevated temperature. In addition, the vibration intensity of C–O (1042 cm^{-1}) in GB produced at 450 °C was lower than that in GM, owing to the removal of the organic compounds, and that of C–O was enhanced due to the decomposition of C=O by deoxidization at elevated pyrolysis temperature.[48] All GB exhibited the typical aromatic –CH peak at 900 to 500 cm^{-1}, attributed to the distorted vibration of the aromatic ring. This observation was also reported by Farobie *et al.*, who found similar peaks associated with aromatic compounds in macroalgae *Sargassum* sp.-derived BC[49] Additionally, the intensity of aromatic –CH increased as the pyrolysis temperature improved. This result confirmed that GB prepared at high temperature possessed higher aromatization degree.

To elucidate the evolution characteristic of functional groups in GM with pyrolysis temperature, the FTIR data was analyzed using two-dimensional correlation spectra (2D-COS) in which the pyrolysis temperature was the external perturbation. The synchronous and asynchronous 2D-COS-FTIR maps in the range of 1750–750 cm^{-1} are shown in Fig. 5b and c, respectively. As shown in Fig. 5b, there were four prominent autocorrelation peaks in the synchronous map, which are located at 1636, 1434, 1039, and 875, respectively. Based on the intensity of the autocorrelation peak, the over susceptibility of functional groups on the GB surface followed the order of aromatic C–H > C=O > CO_3^{2-} > C–O. According to the signals of cross-peak in the synchronous and asynchronous maps, the change order of functional groups for GB in response to elevated pyrolysis temperature followed the sequence CO_3^{2-} > C=O > C–O > aromatic C–H. The 2D-COS-FTIR results indicated that carbonates decomposed first, and then C=O broke into C–O, and finally the surface functional groups condensed to form an aromatic ring in the process of GM pyrolysis.

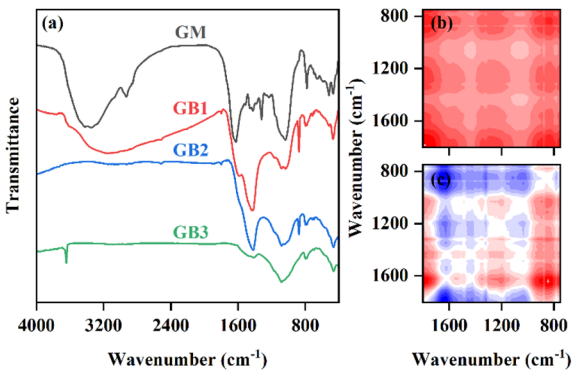

Fig. 5 The FTIR spectra of grub manure (GM) and grub manure-derived biochar (GB) (a). The synchronous (b) and asynchronous (c) 2D-COS maps generated from FTIR spectra. Red and blue indicate the positive and negative correlation, respectively, and higher color intensity indicates stronger correlation. GB1, GB2 and GB3 represent grub manure-derived biochar produced at 450, 600 and 750 °C, respectively.

3.6 Potentially toxic elements

The potentially toxic elements (PTEs) in BC are one of the most concerned inorganic contaminants. The total content of PTEs in GM and GBs is listed in Table S1.† It is worth noting that the total content of PTEs in feedstock increased as follows: Cd (0.09 mg kg^{-1}) < As (5.09 mg kg^{-1}) < Pb (6.54 mg kg^{-1}) < Ni (9.86 mg kg^{-1}) < Cr (10.01 mg kg^{-1}) < Cu (11.05 mg kg^{-1}) < Zn (35.52 mg kg^{-1}). When GM pyrolyzed at 450 and 600 °C, the

total content of Cr, Ni, Zn and Pb in GB increased, while that of Cu, As and Cd decreased. The total content of PTEs in GB1 and GB2 all followed the order of Zn > Cr > Ni > Pb > Cu > As > Cd. With the pyrolysis temperature rising to 750 °C, the total content of PTEs exhibited the following sequence: Zn (141.18 mg kg^{-1}) > Cr (20.45 mg kg^{-1}) > Ni (19.32 mg kg^{-1}) > Cu (13.80 mg kg^{-1}) > Pb (4.00 mg kg^{-1}) > As (3.90 mg kg^{-1}) > Cd (0.09 mg kg^{-1}). Compared with the feedstock, the total content of Cr, Ni, Cu and Zn in GB3 significantly increased by 104.33%, 95.96%, 24.85% and 297.43%, respectively, which resulted from the decomposition of organic compounds in GM.[50] The total content of As, Cd and Pb in GB3 decreased by 23.53%, 70.85%, and 38.79% compared with feedstock, respectively. This result was consistent with a previous study, which was attributed to the formation of volatile chloride compounds at high temperature.[51] Although some PTEs in GM were concentrated after being pyrolyzed, all PTEs in GB met the permissible limits recommended by the International Biochar Initiative.

To assess the leaching behavior of PTEs in GM and GB, the leachable concentration of PTEs was determined using TCLP. As shown in Table S1,† the leachable concentration of Zn in GM was highest among all PTEs. The leachable concentration of PTEs in GM decreased as follows: Zn (3.82 mg kg^{-1}) > As (0.84 mg kg^{-1}) > Cu (0.57 mg kg^{-1}) > Ni (0.12 mg kg^{-1}) > Pb (0.10 mg kg^{-1}) > Cr (0.07 mg kg^{-1}) > Cd (0.02 mg kg^{-1}). In general, pyrolysis of GM suppressed the leachability of PTEs in GBs. The leaching concentration of PTEs in GBs significantly decreased compared with GM. For GB1 and GB2, the leaching content of As all was the highest, being 0.59 and 0.19 mg kg^{-1}, respectively. Remarkably, the leachability of PTEs in GB prepared at 750 °C was extremely decreased. Similar results were also reported by Sun *et al.*,[20] who found that the leaching rate of PTEs in crop straw-derived BC was decreased as the pyrolysis temperature increased. Some PTE compounds could be encapsulated on the developed pore structure of GB, and even form more stable substances (mineral salts or metal–organic complexes), ultimately contributing to poor PTE leaching ability in GB pyrolyzed at high temperature.[17,52]

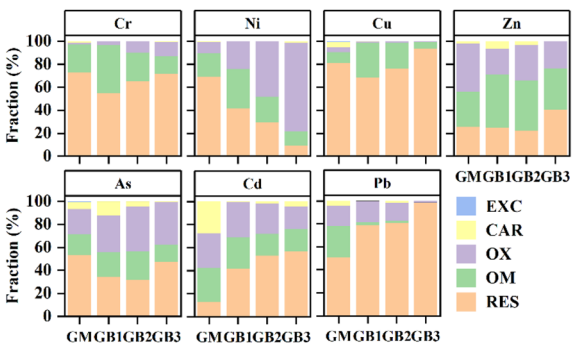

Fig. 6 The fraction of potentially toxic elements for grub manure (GM) and grub manure-derived biochar (GB). GB1, GB2 and GB3 represent grub manure-derived biochar produced at 450, 600 and 750 °C, respectively. EXC, CAR, OX, OM and RES indicate the exchangeable, carbonate bound, Fe–Mn oxide bound, organic matter bound and residual fractions of PTEs, respectively.

The chemical fraction of PTEs in GM and GBs is illustrated in Fig. 6. The main fraction of Cr, Ni, Cu, As and Pb in GM was RES fraction (being 72.75%, 69.10%, 80.96%, 53.32% and 50.66%). The relative content of RES fraction for Cr and Ni in GBs was decreased by 1.00–17.72% and 27.53–59.92%, respectively, whereas the OX fraction of Cr elevated by 1.25–10.57% and 14.16–67.19% compared with GM, respectively. The RES fraction percentage of Cu decreased first and then increased with the increase of pyrolysis temperature. The EXC and CAR fraction of Cu in GM was significantly decreased after it was pyrolyzed. Zn in GM was mainly bound to the OX fraction. The percentage of OX fraction reduced from 41.88% in GM to 22.06–30.45% in GBs. The relative content of EXC, CAR, OX and OM fractions for As in GM was 0.51%, 6.13%, 21.80% and 18.24%, respectively. The EXC fraction of As decreased by 0.48–0.51 and the OX fraction of As in GBs was enhanced with an increase of 10.36–17.33% when compared with the GM. Importantly, the CAR and RES fraction of Cd in GM was 27.53% and 12.57%, respectively, which indicated that Cd in GM showed potential environmental risk when GM was applied to soil.[53] The EXC fraction of Cd in GBs decreased by 23.32–27.25% and the RES fraction of Cd improved by 29.09–43.99%. This result suggested that pyrolysis accelerated the transformation of the EXC fraction of Cd to the RES fraction at elevated temperature, resulting in the decrease of Cd risk. Pb in GBs existed primarily in the form of RES fraction, with the content of 78.59–98.48%, and the RES fraction of Pb in GBs increased as the pyrolysis temperature raised.

The risk evaluation index (REI) of PTEs for GM and GBs is shown in Table 2. According to the REI of PTEs for GM, Cr showed no risk, Ni, Cu, Cd and Pb showed low risk, while Zn and As appeared as medium risk. Hence, the presence of Zn and As in GM posed certain environmental hazards. The REI of Cr, Ni, Cu, Zn, As and Pb was significantly decreased when GM was

Table 2 The total content and leachable concentration of potentially toxic elements (PTEs) for grub manure (GM) and grub manure-derived biochar (GB)[a]

PTEs		GM	GB1	GB2	GB3
TC	Cr	10.01 ± 0.81	16.65 ± 0.39	23.47 ± 2.54	20.45 ± 1.62
	Ni	9.86 ± 1.28	15.97 ± 1.59	19.48 ± 1.56	19.32 ± 0.89
	Cu	11.05 ± 0.31	7.61 ± 1.05	7.72 ± 1.06	13.80 ± 0.95
	Zn	35.52 ± 0.92	61.44 ± 3.49	64.82 ± 3.11	141.18 ± 2.81
	As	5.09 ± 0.15	4.63 ± 0.32	3.99 ± 0.10	3.90 ± 0.05
	Cd	0.31 ± 0.03	0.21 ± 0.01	0.13 ± 0.02	0.09 ± 0.02
	Pb	6.54 ± 0.80	10.16 ± 0.75	10.51 ± 0.62	4.00 ± 0.97
LC	Cr	0.07 ± 0	0.01 ± 0	ND	ND
	Ni	0.12 ± 0.01	0.02 ± 0	0.05 ± 0.01	0.02 ± 0
	Cu	0.57 ± 0.02	0.01 ± 0.01	ND	0.01 ± 0
	Zn	3.82 ± 0.41	ND	ND	ND
	As	0.84 ± 0.02	0.59 ± 0.08	0.19 ± 0.01	0.01 ± 0
	Cd	0.02 ± 0	ND	ND	0.01 ± 0
	Pb	0.10 ± 0	0.01 ± 0	ND	ND

[a] Data are shown as mean ± standard deviation (n = 3). TC: total content (mg kg^{-1}), LC: leachable concentration (mg kg^{-1}). ND: not detected. GB1, GB2 and GB3 represent grub manure-derived biochar produced at 450, 600 and 750 °C, respectively.

Table 3 The risk evaluation index (REI) of potentially toxic elements (PTEs) for grub manure (GM) and grub manure-derived biochar (GB)[a]

	Samples			
REI	GM	GB1	GB2	GB3
Cr	0.75 ± 0.06a	0.03 ± 0.05b	0b	0b
Ni	1.27 ± 0.13a	0.10 ± 0.04b	0.25 ± 0.05b	0.08 ± 0.01b
Cu	5.19 ± 0.12a	0.10 ± 0.11b	0b	0.04 ± 0.01b
Zn	10.76 ± 1.13a	0b	0b	0b
As	16.52 ± 0.52a	12.75 ± 2.25b	4.81 ± 0.23c	0.33 ± 0.05d
Cd	6.03 ± 0.49b	2.04 ± 0.63c	3.54 ± 0.82c	8.18 ± 1.85a
Pb	1.62 ± 0.17a	0.02 ± 0.04b	0b	0b

[a] Data are shown as mean ± standard deviation ($n = 3$). No risk, REI ≤ 1%; low risk, 1% ≤ REI ≤ 10%; medium risk, 11% ≤ REI ≤ 30%; high risk, 31% ≤ REI ≤ 50%; and very high risk, REI > 50%. Data are shown as mean ± standard deviation ($n = 3$). GB1, GB2 and GB3 represent grub manure-derived biochar produced at 450, 600 and 750 °C. Different letters indicate significant differences between different treatments ($P < 0.05$).

pyrolyzed Table 3. The environmental risk of Ni, Cu, Zn, As and Pb changed from low or medium risk (1.27–16.52) to no risk (0–0.33). Notably, the REI of Cd for GB1 and GB2 was significantly decreased compared with GM by 3.99 and 2.49, respectively, but the REI of Cd for GB3 was 2.15 higher that of GM. However, the Cd in GB3 appeared still as low risk. In conclusion, the pyrolysis of GM to GB could effectively reduce the potential environmental hazards of PTEs in GM, which was in line with the previous research. These results were in line with the previous research reported by Wang *et al.*, who found that the potential ecotoxicity of PTEs in cow manure BC reduced and environmental safety improved with the pyrolysis temperature.[54]

4 Conclusion

Pyrolysis is a sustainable alternative method to achieve rational treatment of GM and obtain high-value products (biochar). Pyrolysis temperature significantly affects the elemental composition, microstructure feature, thermal stability, surface functionality and potential environmental risk of GB. The GB produced at low pyrolysis temperature, which possessed rich nutrient content and surface functional groups, may be suitable for improving soil fertility and adsorbing heavy metal contaminants. The GB prepared at high pyrolysis temperature showed the highest carbon content, aromatization degree, stability and specific surface area, which not only can achieve carbon sequestration, but also demonstrated the potential to remove organic contaminants. In addition, pyrolysis significantly reduces the hazards of PTEs in GM, but the potential environmental risks of Cd in GB produced at high temperature still need to be paid attention to. Overall, this study would provide a prospective guidance for the eco-friendly utilization of grub manure, and the potential agricultural and environmental applications of grub manure-derived biochar. Although grub manure-derived biochar has tremendous potential for various applications, advanced techniques are needed to characterize the relationship between the biochar structure and pyrolysis processes in the future, and pyrolysis technology and reaction equipment also need to be optimized for future large-scale production.

Data availability

The authors will supply the relevant data in response to reasonable requests.

Conflicts of interest

The authors declare that they have no competing interests.

Acknowledgements

This work was supported by the This work was supported by the National Natural Science Foundation of China (42307056), the fund for Shanxi "1331 Project" Key Subjects Construction (1331KSC) and the Technological Innovation Programs of Higher Education Institutions in Shanxi (2021L523, 2023L329).

References

1 K. Wang, P. Gao, L. Geng, C. Liu, J. Zhang and C. Shu, Lignocellulose degradation in *Protaetia brevitarsis* larvae digestive tract: Refining on a tightly designed microbial fermentation production line, *Microbiome*, 2022, **10**, 90, DOI: 10.1186/s40168-022-01291-2.

2 B. Du, H. Xuan, L. Geng, W. Li, J. Zhang, W. Xiang, R. Liu and C. Shu, Microflora for improving the Auricularia auricula spent mushroom substrate for *Protaetia brevitarsis* production, *iScience*, 2022, **25**, 105307, DOI: 10.1016/j.isci.2022.105307.

3 Y. Li, T. Fu, L. Geng, Y. Shi, H. Chu, F. Liu, C. Liu, F. Song, J. Zhang and C. Shu, *Protaetia brevitarsis* larvae can efficiently convert herbaceous and ligneous plant residues to humic acids, *Waste Manage.*, 2019, **83**, 79–82, DOI: 10.1016/j.wasman.2018.11.010.

4 H. Xuan, P. Gao, B. Du, L. Geng, K. Wang, K. Huang, J. Zhang, T. Huang and C. Shu, Characterization of microorganisms from *Protaetia brevitarsis* Larva frass, *Microorganisms*, 2022, **10**, 311, DOI: 10.3390/microorganisms10020311.

5 K. H. Joung, J.-W. Kim, S.-B. Lee, D. H. Jang, B.-M. Yoo, S.-M. Bea, Y. H. Chang, Y. H. Lee and D. C. Seo, Effects of protaetia *brevitarsis larvae* manure application on lettuce growth and soil chemical properties, *Korean J. Soil Sci. Fert.*, 2022, **55**, 80–85, DOI: 10.7745/KJSSF.2022.55.1.080.

6 G. Su, H. C. Ong, N. W. Mohd Zulkifli, S. Ibrahim, W. H. Chen, C. T. Chong and Y. S. Ok, Valorization of animal manure via pyrolysis for bioenergy: A review, *J. Cleaner Prod.*, 2022, **343**, 130965, DOI: 10.1016/j.jclepro.2022.130965.

7 D. T. N. Wijesinghe, H. C. Suter, P. J. Scales and D. Chen, Lignite addition during anaerobic digestion of ammonium rich swine manure enhances biogas production, *J. Environ.*

Chem. Eng., 2021, **9**, 104669, DOI: **10.1016/j.jece.2020.104669**.

8 M. He, Z. Xu, D. Hou, B. Gao, X. Cao, Y. S. Ok, J. Rinklebe, N. S. Bolan and D. C. W. Tsang, Waste-derived biochar for water pollution control and sustainable development, *Nat. Rev. Earth Environ.*, 2022, **3**, 444–460, DOI: **10.1038/s43017-022-00306-8**.

9 J. Lehmann, A. Cowie, C. A. Masiello, C. Kammann, D. Woolf, J. E. Amonette, M. L. Cayuela, M. Camps-Arbestain and T. Whitman, Biochar in climate change mitigation, *Nat. Geosci.*, 2021, **14**, 883–892, DOI: **10.1038/s41561-021-00852-8**.

10 P. Wu, S. T. Ata-Ul-Karim, B. P. Singh, H. Wang, T. Wu, C. Liu, G. Fang, D. Zhou, Y. Wang and W. Chen, A scientometric review of biochar research in the past 20 years (1998–2018), *Biochar*, 2019, **1**, 23–43, DOI: **10.1007/s42773-019-00002-9**.

11 C. Yan, T. Sun, H. Jia, Y. Xu and Y. Sun, Characterization of chicken manure biochar relevant to its potential use in remediation of Cd contaminated water, *Desalin. Water Treat.*, 2021, **221**, 197–206, DOI: **10.5004/dwt.2021.27022**.

12 P. Zhang, X. Zhang, X. Yuan, R. Xie and L. Han, Characteristics, adsorption behaviors, Cu(II) adsorption mechanisms by cow manure biochar derived at various pyrolysis temperatures, *Bioresour. Technol.*, 2021, **331**, 125013, DOI: **10.1016/j.biortech.2021.125013**.

13 S. Wei, M. Zhu, X. Fan, J. Song, P. a. Peng, K. Li, W. Jia and H. Song, Influence of pyrolysis temperature and feedstock on carbon fractions of biochar produced from pyrolysis of rice straw, pine wood, pig manure and sewage sludge, *Chemosphere*, 2019, **218**, 624–631, DOI: **10.1016/j.chemosphere.2018.11.177**.

14 X. Yang, W. Ng, B. S. E. Wong, G. H. Baeg, C.-H. Wang and Y. S. Ok, Characterization and ecotoxicological investigation of biochar produced via slow pyrolysis: Effect of feedstock composition and pyrolysis conditions, *J. Hazard. Mater.*, 2019, **365**, 178–185, DOI: **10.1016/j.jhazmat.2018.10.047**.

15 K. B. Cantrell, P. G. Hunt, M. Uchimiya, J. M. Novak and K. S. Ro, Impact of pyrolysis temperature and manure source on physicochemical characteristics of biochar, *Bioresour. Technol.*, 2012, **107**, 419–428, DOI: **10.1016/j.biortech.2011.11.084**.

16 X. Shen, J. Zeng, D. Zhang, F. Wang, Y. Li and W. Yi, Effect of pyrolysis temperature on characteristics, chemical speciation and environmental risk of Cr, Mn, Cu, and Zn in biochars derived from pig manure, *Sci. Total Environ.*, 2020, **704**, 135283, DOI: **10.1016/j.scitotenv.2019.135283**.

17 P. Zhang, X. Zhang, Y. Li and L. Han, Influence of pyrolysis temperature on chemical speciation, leaching ability, and environmental risk of heavy metals in biochar derived from cow manure, *Bioresour. Technol.*, 2020, **302**, 122850, DOI: **10.1016/j.biortech.2020.122850**.

18 O. Farobie, A. Amrullah, N. Syaftika, A. Bayu, E. Hartulistiyoso, W. Fatriasari and A. B. Dani Nandiyanto, Valorization of rejected macroalgae *Kappaphycopsis cottonii* for bio-oil and bio-char production via slow pyrolysis, *ACS Omega*, 2024, **9**, 16665–16675, DOI: **10.1021/acsomega.4c00678**.

19 Z. Liu, M. Jia, Q. Li, S. Lu, D. Zhou, L. Feng, Z. Hou and J. Yu, Comparative analysis of the properties of biochars produced from different pecan feedstocks and pyrolysis temperatures, *Ind. Crops Prod.*, 2023, **197**, 116638, DOI: **10.1016/j.indcrop.2023.116638**.

20 T. Sun, Y. Sun, Q. Huang, Y. Xu and H. Jia, Sustainable exploitation and safe utilization of biochar: Multiphase characterization and potential hazard analysis, *Bioresour. Technol.*, 2023, **383**, 129241, DOI: **10.1016/j.biortech.2023.129241**.

21 A. Tessier, P. G. C. Campbell and M. Bisson, Sequential extraction procedure for the speciation of particulate trace metals, *Anal. Chem.*, 1979, **51**, 844–851, DOI: **10.1021/ac50043a017**.

22 K. B. Cantrell, P. G. Hunt, M. Uchimiya, J. M. Novak and K. S. Ro, Impact of pyrolysis temperature and manure source on physicochemical characteristics of biochar, *Bioresour. Technol.*, 2012, **107**, 419–428, DOI: **10.1016/j.biortech.2011.11.084**.

23 F. Lian and B. Xing, Black carbon (biochar) in water/soil environments: Molecular structure, sorption, stability, and potential risk, *Environ. Sci. Technol.*, 2017, **51 23**, 13517–13532, DOI: **10.1021/acs.est.7b02528**.

24 Y.-K. Choi, T.-R. Choi, R. Gurav, S. K. Bhatia, Y.-L. Park, H. J. Kim, E. Kan and Y.-H. Yang, Adsorption behavior of tetracycline onto *Spirulina sp*. (microalgae)-derived biochars produced at different temperatures, *Sci. Total Environ.*, 2020, **710**, 136282, DOI: **10.1016/j.scitotenv.2019.136282**.

25 R. K. Mishra and K. Mohanty, Bio-oil and biochar production using thermal and catalytic pyrolysis of low-value waste neem seeds over low-cost catalysts: effects of operating conditions on product yields and studies of physicochemical characteristics of bio-oil and biochar, *Biochar*, 2021, **3**, 641–656, DOI: **10.1007/s42773-021-00105-2**.

26 R. K. Mishra and K. Mohanty, Pyrolysis of low-value waste sawdust over low-cost catalysts: physicochemical characterization of pyrolytic oil and value-added biochar, *Biofuel Res. J.*, 2022, **9**, 1736–1749, DOI: **10.18331/BRJ2022.9.4.4**.

27 Z. Khanmohammadi, M. Afyuni and M. R. Mosaddeghi, Effect of pyrolysis temperature on chemical and physical properties of sewage sludge biochar, *Waste Manage. Res.*, 2015, **33**, 275–283, DOI: **10.1177/0734242x14565210**.

28 B. Zhao, D. O'Connor, J. Zhang, T. Peng, Z. Shen, D. C. W. Tsang and D. Hou, Effect of pyrolysis temperature, heating rate, and residence time on rapeseed stem derived biochar, *J. Cleaner Prod.*, 2018, **174**, 977–987, DOI: **10.1016/j.jclepro.2017.11.013**.

29 J. W. Lee, M. Kidder, B. R. Evans, S. Paik, A. C. Buchanan Iii, C. T. Garten and R. C. Brown, Characterization of biochars produced from cornstovers for soil amendment, *Environ. Sci. Technol.*, 2010, **44**, 7970–7974, DOI: **10.1021/es101337x**.

30 D. V. Cuong, P.-C. Wu, L.-I. Chen and C.-H. Hou, Active MnO_2/biochar composite for efficient As(III) removal:

Insight into the mechanisms of redox transformation and adsorption, *Water Res.*, 2021, **188**, 116495, DOI: 10.1016/j.watres.2020.116495.

31 K. K. B. Suresh Babu, M. Nataraj, M. Tayappa, Y. Vyas, R. K. Mishra and B. Acharya, Production of biochar from waste biomass using slow pyrolysis: Studies of the effect of pyrolysis temperature and holding time on biochar yield and properties, *Mater. Sci. Energy Technol.*, 2024, **7**, 318–334, DOI: 10.1016/j.mset.2024.05.002.

32 Q. Li, S. Zhang, M. Gholizadeh, X. Hu, X. Yuan, B. Sarkar, M. Vithanage, O. Mašek and Y. S. Ok, Co-hydrothermal carbonization of swine and chicken manure: Influence of cross-interaction on hydrochar and liquid characteristics, *Sci. Total Environ.*, 2021, **786**, 147381, DOI: 10.1016/j.scitotenv.2021.147381.

33 S. K. Das, G. K. Ghosh, R. K. Avasthe and K. Sinha, Compositional heterogeneity of different biochar: Effect of pyrolysis temperature and feedstocks, *J. Environ. Manage.*, 2021, **278**, 111501, DOI: 10.1016/j.jenvman.2020.111501.

34 L. Zhao, X. Cao, O. Mašek and A. Zimmerman, Heterogeneity of biochar properties as a function of feedstock sources and production temperatures, *J. Hazard. Mater.*, 2013, **256–257**, 1–9, DOI: 10.1016/j.jhazmat.2013.04.015.

35 T. Sun, Y. Xu, Y. Sun, L. Wang, X. Liang and H. Jia, Crayfish shell biochar for the mitigation of Pb contaminated water and soil: Characteristics, mechanisms, and applications, *Environ. Pollut.*, 2021, **271**, 116308, DOI: 10.1016/j.envpol.2020.116308.

36 X. Xiao and B. Chen, A direct observation of the fine aromatic clusters and molecular structures of biochars, *Environ. Sci. Technol.*, 2017, **51**, 5473–5482, DOI: 10.1021/acs.est.6b06300.

37 T. Sun, P. Pei, Y. Sun, Y. Xu and H. Jia, Performance and mechanism of As(III/V) removal from aqueous solution by novel positively charged animal-derived biochar, *Sep. Purif. Technol.*, 2022, **290**, 120836, DOI: 10.1016/j.seppur.2022.120836.

38 J. Hu, Y. Shen and N. Zhu, Optimizing adsorption performance of sludge-derived biochar via inherent moisture-regulated physicochemical properties, *Waste Manage.*, 2023, **169**, 70–81, DOI: 10.1016/j.wasman.2023.06.033.

39 R. Kumar Mishra, D. Jaya Prasanna Kumar, A. Narula, S. Minnat Chistie and S. Ullhas Naik, Production and beneficial impact of biochar for environmental application: A review on types of feedstocks, chemical compositions, operating parameters, techno-economic study, and life cycle assessment, *Fuel*, 2023, **343**, 127968, DOI: 10.1016/j.fuel.2023.127968.

40 R. K. Mishra and K. Mohanty, A review of the next-generation biochar production from waste biomass for material applications, *Sci. Total Environ.*, 2023, **904**, 167171, DOI: 10.1016/j.scitotenv.2023.167171.

41 J. Bu, B.-B. Hu, H.-Z. Wu and M.-J. Zhu, Improved methane production with redox-active/conductive biochar amendment by establishing spatial ecological niche and mediating electron transfer, *Bioresour. Technol.*, 2022, **351**, 127072, DOI: 10.1016/j.biortech.2022.127072.

42 Y. Wang, K. Wang, X. Wang, Q. Zhao, J. Jiang and M. Jiang, Effect of different production methods on physicochemical properties and adsorption capacities of biochar from sewage sludge and kitchen waste: Mechanism and correlation analysis, *J. Hazard. Mater.*, 2024, **461**, 132690, DOI: 10.1016/j.jhazmat.2023.132690.

43 L. Leng, S. Xu, R. Liu, T. Yu, X. Zhuo, S. Leng, Q. Xiong and H. Huang, Nitrogen containing functional groups of biochar: An overview, *Bioresour. Technol.*, 2020, **298**, 122286, DOI: 10.1016/j.biortech.2019.122286.

44 W. Yu, F. Lian, G. Cui and Z. Liu, N-doping effectively enhances the adsorption capacity of biochar for heavy metal ions from aqueous solution, *Chemosphere*, 2018, **193**, 8–16, DOI: 10.1016/j.chemosphere.2017.10.134.

45 H. Li, M. Tang, X. Huang, L. Wang, Q. Liu and S. Lu, An efficient biochar adsorbent for CO_2 capture: Combined experimental and theoretical study on the promotion mechanism of N-doping, *Chem. Eng. J.*, 2023, **466**, 143095, DOI: 10.1016/j.cej.2023.143095.

46 M. Fan, C. Li, Y. Shao, S. Zhang, M. Gholizadeh and X. Hu, Pyrolysis of cellulose: Correlation of hydrophilicity with evolution of functionality of biochar, *Sci. Total Environ.*, 2022, **825**, 153959, DOI: 10.1016/j.scitotenv.2022.153959.

47 M. Fan, C. Li, Y. Sun, L. Zhang, S. Zhang and X. Hu, In situ characterization of functional groups of biochar in pyrolysis of cellulose, *Sci. Total Environ.*, 2021, **799**, 149354, DOI: 10.1016/j.scitotenv.2021.149354.

48 C. Zhang, L. Chao, Z. Zhang, L. Zhang, Q. Li, H. Fan, S. Zhang, Q. Liu, Y. Qiao, Y. Tian, Y. Wang and X. Hu, Pyrolysis of cellulose: Evolution of functionalities and structure of bio-char versus temperature, *Renewable Sustainable Energy Rev.*, 2021, **135**, 110416, DOI: 10.1016/j.rser.2020.110416.

49 O. Farobie, A. Amrullah, A. Bayu, N. Syaftika, L. A. Anis and E. Hartulistiyoso, In-depth study of bio-oil and biochar production from macroalgae *Sargassum* sp. via slow pyrolysis, *RSC Adv.*, 2022, **12**, 9567–9578, DOI: 10.1039/D2RA00702A.

50 J. Lin, C. Cui, S. Sun, R. Ma, W. Yang and Y. Chen, Synergistic optimization of syngas quality and heavy metal immobilization during continuous microwave pyrolysis of sludge: Competitive relationships, reaction mechanisms, and energy efficiency assessment, *J. Hazard. Mater.*, 2022, **438**, 129451, DOI: 10.1016/j.jhazmat.2022.129451.

51 L. Wang, D. O'Connor, J. Rinklebe, Y. S. Ok, D. C. W. Tsang, Z. Shen and D. Hou, Biochar aging:M echanisms, physicochemicalchanges, assessment, and implications for field applications, *Environ. Sci. Technol.*, 2020, **54**, 14797–14814, DOI: 10.1021/acs.est.0c04033.

52 A. Raj, A. Yadav, S. Arya, R. Sirohi, S. Kumar, A. P. Rawat, R. S. Thakur, D. K. Patel, L. Bahadur and A. Pandey, Preparation, characterization and agri applications of biochar produced by pyrolysis of sewage sludge at different temperatures, *Sci. Total Environ.*, 2021, **795**, 148722, DOI: 10.1016/j.scitotenv.2021.148722.

53 Z. Fan, X. Zhou, Z. Peng, S. Wan, Z. F. Gao, S. Deng, L. Tong, W. Han and X. Chen, Co-pyrolysis technology for enhancing the functionality of sewage sludge biochar and immobilizing heavy metals, *Chemosphere*, 2023, **317**, 137929, DOI: **10.1016/j.chemosphere.2023.137929**.

54 X. Wang, C. Li, Z. Li, G. Yu and Y. Wang, Effect of pyrolysis temperature on characteristics, chemical speciation and risk evaluation of heavy metals in biochar derived from textile dyeing sludge, *Ecotoxicol. Environ. Saf.*, 2019, **168**, 45–52, DOI: **10.1016/j.ecoenv.2018.10.022**.